SCIENCE CHINA
Chemistry

•ARTICLES•

July 2020 Vol.63 No.7: 997–1003
https://doi.org/10.1007/s11426-020-9743-2

Construction of MoS_2 field effect transistor sensor array for the detection of bladder cancer biomarkers

Yujie Yang[1†], Bo Zeng[1†], Yingxue Li[1], Huageng Liang[3], Yanbing Yang[1,2,4*] & Quan Yuan[1,2*]

[1]*Key Laboratory of Analytical Chemistry for Biology and Medicine (Ministry of Education), College of Chemistry and Molecular Sciences, Wuhan University, Wuhan 430072, China;*
[2]*Institute of Chemical Biology and Nanomedicine, State Key Laboratory of Chemo/Biosensing and Chemometrics, College of Chemistry and Chemical Engineering, Hunan University, Changsha 410082, China;*
[3]*Department of Urology, Union Hospital, Tongji Medical College, Huazhong University of Science and Technology, Wuhan 430022, China;*
[4]*Key Laboratory for Micro-/Nano-Optoelectronic Devices of Ministry of Education, School of Physics and Electronics, Hunan University, Changsha 410082, China*

Received February 4, 2020; accepted April 13, 2020; published online May 14, 2020

Bladder cancer is one of the commonest malignant tumors of urinary system with high recurrence. However, currently developed bladder cancer urine diagnosis methods are hindered by the low detection sensitivity and accuracy. Herein, a molybdenum disulfide (MoS_2) nanosheets-based field effect transistor (FET) sensor array was constructed for simultaneous detection of multiple bladder cancer biomarkers in human urine. With the excellent electronic property of MoS_2 and the high specific identification capability of recognition molecules, the proposed biosensor array could simultaneously detect nuclear matrix protein 22 (NMP22) and cytokeratin 8 (CK8) with a wide linear range of 10^{-6}–10^{-1} pg mL^{-1} and an ultra-low detection limit of 0.027 and 0.019 aM, respectively. Furthermore, this highly sensitive and specific MoS_2 FET sensor array could be used to identify bladder cancer biomarkers from human urine samples. This designed high-performance biosensor array shows great potential in the future diagnosis of bladder cancer.

MoS_2, field effect transistor, bladder cancer, sensor array, NMP22, CK8

Citation: Yang Y, Zeng B, Li Y, Liang H, Yang Y, Yuan Q. Construction of MoS_2 field effect transistor sensor array for the detection of bladder cancer biomarkers. *Sci China Chem*, 2020, 63: 997–1003, https://doi.org/10.1007/s11426-020-9743-2

1 Introduction

As one of the commonest malignant tumors in the urinary system, the incidence of bladder cancer is the second highest in the urological malignancies [1,2]. Currently, cystoscopy and tissue biopsy are the gold standards for bladder cancer diagnosis, while these processes bring great pains to patients due to its high invasiveness [3,4]. Recently, liquid biopsy has been considered as alternative candidates of cystoscopy and tissue biopsy in clinical diagnosis benefiting from its prominent characteristics such as non-invasiveness and the ability to avoid diagnosis deviation originated from tissue heterogeneity [5–7]. Liquid biopsy could detect disease biomarkers from various kinds of body fluids such as blood, urine, saliva, and sweat [8–11]. As we know, bladder is a human organ with urine storage capability and the metabolic environment of bladder is urine, thus the occurrence and development of bladder cancer is closely relevant to the components of urine [12]. In this regard, bladder cancer urine diagnosis would bring hope for non-invasive early-stage bladder cancer diagnosis. Recently, the optical and electro-

†These authors contributed equally to this work.
*Corresponding authors (email: yangyanbing@whu.edu.cn; yuanquan@whu.edu.cn)

chemical biosensors have been developed to detect a series of bladder cancer urinary biomarkers such as bladder tumor associated antigen, nuclear matrix protein 22 (NMP22), the cytokeratins (CKs) and telomerase [13–20]. However, the composition of urine is very complex and currently developed liquid biopsy diagnosis methods rely on the detection of a single biomarker with low detection sensitivity and accuracy [21,22]. To this end, the development of an efficient approach to enable the simultaneous sensitive detection of multiple bladder tumor biomarkers is extremely necessary to realize the diagnosis of bladder cancer.

Field effect transistor (FET) is an electrical device which is composed of source/drain electrodes and semiconductor channel materials [23]. The FET electrical sensors exhibit prominent characteristics such as high sensitivity, ultra-fast response, and low limit of detection [24]. Owing to these advantages, FET-based biosensors constructed from carbon nanotubes, Si nanowires, graphene and transition-metal dichalcogenides have been developed to detect a range of disease biomarkers such as viruses, cancer biomarkers, small molecules, and pathogens [25–28]. Among the nanomaterials used to build FET biosensors, molybdenum disulfide (MoS_2) exhibits excellent electrical properties including a direct bandgap, an excellent on/off ratio and high carrier mobilities at room temperature [29,30]. Besides, the well-developed chemical vapor deposition (CVD) provides a controlled method to grow high-quality and large-area MoS_2 nanosheets at a reasonable cost [31]. By controlling the materials synthesis and device fabrication processes, a MoS_2 FET sensor array with multi-channel sensing units that are capable of detecting multiple biomarkers could be constructed to increase the detection sensitivity and accuracy [32].

In this work, we constructed a MoS_2 nanosheets-based FET sensor array for the simultaneous detection of two types of bladder cancer biomarkers in human urine with high sensitivity, specificity and accuracy (Scheme 1). Specifically, two types of recognition molecules with high specific binding affinity to specific biomarkers were conjugated on different MoS_2 nanosheets sensing channels to achieve simultaneous detection. The specific binding of target biomarkers to the recognition molecules functionalized MoS_2 device would cause an obvious change in the channel current, consequently achieving quantitative detection of two types of biomarkers. Because of the excellent electrical characteristics of MoS_2 and the high specific identification capability of recognition molecules, the MoS_2 FET biosensor array can reliably detect bladder cancer biomarkers NMP22 and cytokeratin 8 (CK8) with an ultralow detection limit of 0.027 and 0.019 aM, respectively. More importantly, the MoS_2 FET sensor array could also realize highly sensitive and specific capture and detection of bladder cancer biomarkers from human urine samples, demonstrating that the rationally designed multi-channel sensor array could be routinely used for the detection of complex samples with high sensitivity and accuracy. Our design of high performance MoS_2 FET biosensor array for the detection of bladder cancer biomarkers suggests a potential strategy for the achievement of personalized healthcare.

2 Experimental

2.1 Materials and reagents

Ethyl alcohol, acetone, anisole, glutaraldehyde solution, potassium hydroxide, polymethyl methacrylate (PMMA), (3-aminopropyl)-triethoxysilane (APTES) and methyl methacrylate were purchased from Sinopharm Chemical Reagent Co., Ltd. (China). Bovine serum albumin (BSA) and phosphate buffer saline (PBS, 1×, pH 7.4) were bought from Shanghai Yuanye Bio-Technology Co., Ltd. (China). RIPA cell lysis buffer was purchased from Shanghai EpiZyme Biotechnology Co., Ltd. (China). NMP22, anti-NMP22, CK8 and ani-CK8 were purchased from Abcam (Shanghai) Trade Co., Ltd. (China). The MoS_2 nanosheets were provided by Shanghai OnWay Technology Co., Ltd. (China). All the human urine samples of bladder cancer patients and healthy donors were provided by Union Hospital of Wuhan and Wuhan University (China). All three bladder cancer patients belong to non-muscle invasive bladder urothelial carcinoma. Bladder cancer patients No. 1–3 were carcinoma *in situ* (Stage pTis), low-grade papillary urothelial carcinoma

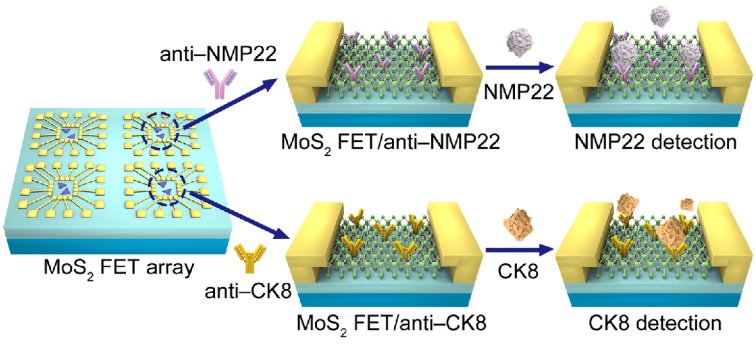

Scheme 1 Schematic illustration of MoS_2 nanosheets-based FET sensor array for simultaneous detection of NMP22 and CK8 (color online).

(Stage pT1) and high-grade papillary urothelial carcinoma (Stage pT1), respectively. Ultrapure water was used throughout the experiment.

Ethical approval: All procedures performed in studies involving human participants were in accordance with the ethical standards of the institutional and/or national research committee and with the 1964 Helsinki declaration and its later amendments or comparable ethical standards.

2.2 Instruments

The morphology of MoS_2 nanosheets is characterized by an optical microscope (Olympus BX1M, Japan) and a scanning electron microscope (SEM; Zeiss Merlin Compact, England). The height of the MoS_2 nanosheet was measured using an atomic force microscopy (AFM; Bruker Dimension ICON, USA). Raman spectra were recorded using a microscopic confocal Raman spectrometer (Renishaw inVia + Plus, England) with a 532 nm laser. The source/drain electrodes array was prepared by an electron beam lithography system (JEOL 6510 with NPGS, Japan) and an ultra violet lithography device (ABM. Inc., USA). Thermal evaporation was performed by a thermal evaporation device (Jiashuo JSD-300, China). The electrical characteristics of MoS_2 FET were tested by a semiconductor analyzer (Agilent 4156B, USA).

2.3 Transfer of MoS_2

The MoS_2 transfer method is improved according to a previously reported method [33]. Specifically, a drop of 4% PMMA anisole solution was dropped on the MoS_2 nanosheets grown on the SiO_2/Si substrate and the substrate was heated to 100 °C to promote the curing of PMMA/MoS_2 film. Then, the PMMA/MoS_2 layer was detached from the substrate by exposing the substrate into a bath of 0.2 M KOH solution to etch the SiO_2 for 1 h. After that, the PMMA/MoS_2 membrane was cleaned with deionized water three times to remove residual KOH and transferred onto the sensing window of the target substrate with prefabricated electrode patterns. Finally, the target substrate was heated to 80 °C to strengthen the binding force between MoS_2 and substrate. The MoS_2 FET array was then obtained after removing the PMMA layer with acetone.

2.4 Fabrication of MoS_2 FET sensor array and bladder cancer biomarkers detection

The functionalization of antibodies was only performed on the active channel surface to improve the detection sensitivity and avoid signal interference. We first passivated the source/drain electrodes by spin-coating a layer of PMMA onto the array and opened an 8 μm×8 μm sensing area in the channel using electron beam lithography [27]. Then, the device was functionalized with APTES and glutaraldehyde as reported [34]. After that, 10 μL anti-NMP22 solution (50 μg mL^{-1}) and 10 μL anti-CK8 solution (2 μg mL^{-1}) were dropped on different sensing windows of the device respectively and the device was incubated at 4 °C overnight to facilitate the efficient functionalization. In the end, 10 μL BSA solution (0.01 g mL^{-1}) was dropped onto the sensing windows for 1 h at 4 °C to passivate the sensing surface and reduce nonspecific adsorption [21]. As for the NMP22 and CK8 detection, the sample solution was dropped on the sensing windows for 5 min to ensure that the association/dissociation reaction between antigen and antibody reaches equilibrium. Then, the electrical sensing performance was measured after rinsing the device with PBS three times to remove unreacted proteins and drying with nitrogen.

2.5 Pretreatment of human urine samples

The urine pretreatment method was adopted according to a previously reported method [35]. Specifically, urine samples collected from bladder cancer patients and healthy donors were centrifuged for 10 min at 850×*g* and 4 °C and the supernatant was discarded. Then, the samples were washed with PBS and centrifuged for 5 min at 2,300×*g* and 4 °C to collect the precipitation. It is worth mentioning that the collection of precipitation is used to ensure efficient cell lysis in the next step and reduce the matrix interference originated from supernatant. Subsequently, 200 μL iced lysis buffer was added into each sample and the samples were incubated on an ice bath for 30 min. The bladder tumor cells in the precipitate were lysed and protein biomarkers were released. In the end, the samples were centrifuged for 20 min at 10,000×*g* and 4 °C, and the supernatant with protein biomarkers was collected and stored at −80 °C for further detection. When detecting the bladder cancer biomarkers in the urine sample, the pretreated samples were diluted 10^6× with PBS.

3 Results and discussion

3.1 Characterization of MoS_2 nanosheets

The CVD grown MoS_2 nanosheets were used for the preparation of MoS_2 sensor array devices. Figure 1(a, b) and Figure S1 (Supporting information online) show the optical micrographs and SEM images of MoS_2 nanosheets, respectively. It can be seen that the MoS_2 triangular crystals with uniform sizes are evenly deposited on a SiO_2/Si substrate. The side length of each MoS_2 triangular crystal is about 20 μm, and this large dimension facilitates the efficient functionalization of recognition molecules. Figure 1(c) shows the AFM image and the corresponding quantitative

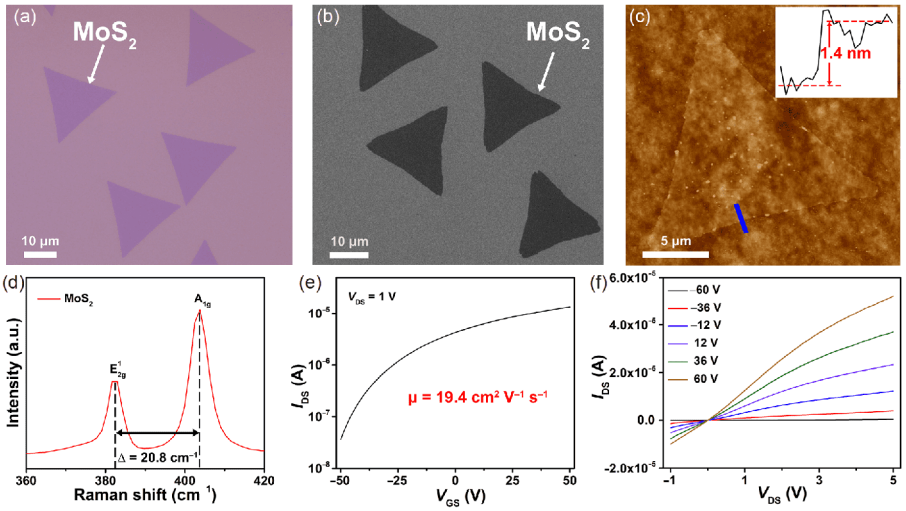

Figure 1 (a) Optical micrograph and (b) SEM image of the MoS_2 nanosheets. (c) AFM image of the MoS_2 nanosheet. Inset: the corresponding quantitative height profile of the MoS_2 nanosheet. (d) Raman spectrum of the MoS_2 nanosheet. (e) Transfer characteristic curve of MoS_2 FET (V_{DS}=1 V). (f) Output characteristic curve of MoS_2 FET (V_{GS}, from −60 to 60 V, step=14 V) (color online).

height profile of a single MoS_2 nanosheet. The measured thickness of the MoS_2 nanosheet is approximately 1.4 nm, indicating that the MoS_2 nanosheet is composed of two stacked MoS_2 layers [36,37]. Additionally, the Raman shift difference of 20.8 cm^{-1} between E^1_{2g} and A_{1g} peaks also verifies that the material prepared is bilayer MoS_2 nanosheet (Figure 1(d)) [38]. This thin MoS_2 nanosheet is beneficial for the large carrier concentration variation and thus the high sensitivity of the biosensor [39]. The electrical characteristics of the back-gated MoS_2 FET were tested with a SiO_2 gate dielectric layer. The transfer characteristic curve (Figure 1(e)) shows that the drain current (I_{DS}) increases with the increase of back-gate bias voltage (V_{GS}) under a given drain-source voltage (V_{DS}=1 V), consistent with the characteristics of n-type semiconductors [40]. The mobility and on/off current ratio of the MoS_2 FET were determined to be 19.4 $cm^2\ V^{-1}\ s^{-1}$ and 10^2, respectively. The output characteristic curve (Figure 1(f)) demonstrates the linearity between I_{DS} and V_{DS}, suggesting the excellent contact between the electrodes and MoS_2 nanosheet.

3.2 Construction of MoS_2 FET sensor array

To fabricate the MoS_2 FET sensor array, we first prepared the Cr/Au electrode patterns on SiO_2 (300 nm)/Si substrate by photolithography and thermal evaporation as shown in Figure 2(a). The device was comprised of an array of four sensing windows, each of which could be used to detect a kind of biomarker without interference from each other. Then, the CVD grown MoS_2 nanosheets were transferred to the middle region of the sensing windows with the assistance of a PMMA polymer layer. Subsequently, the source/drain electrodes were prepared in contact with MoS_2 nanosheets to build FET channels by electron beam lithography and thermal evaporation, as displayed in Figure 2(b). It is worth mentioning that several parallel MoS_2 FET sensing units could be fabricated in each sensing window to enable a multi-channel biosensor and minimize the detection variation of one sensing window. Next, in order to explore the ability of the MoS_2 FET sensor array to detect bladder cancer biomarkers, we modified two specific antibody molecules (anti-NMP22 and anti-CK8) correspondence to FDA-approved bladder cancer biomarkers (NMP22 and CK8) on the FET channels [41,42]. The successful surface functionalization of antibody molecules can be validated by the three-dimensional AFM images of anti-NMP22 and anti-CK8 immobilized MoS_2 nanosheets (Figure S2). From the AFM images, it can be seen that the heights of the anti-NMP22 and anti-CK8 modified MoS_2 nanosheets increase to 6.1 and 10.3 nm, which is higher than that of MoS_2 nanosheets.

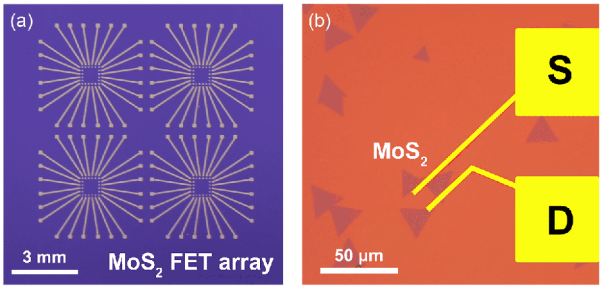

Figure 2 (a) Photograph of the electrode array on the SiO_2/Si substrate. (b) Magnified optical micrograph image of MoS_2 FET device (color online).

3.3 Detection of bladder cancer biomarkers

The detection of NMP22 and CK8 molecules were carried out on two different sensing windows of MoS_2 FET sensor

array and the corresponding I_{DS}-V_{GS} response curves are shown in Figure 3(a, b). It can be observed that as the concentrations of NMP22 and CK8 increase from 10^{-15} to 10^{-9} mg mL^{-1}, the I_{DS} of MoS_2 FET/anti-NMP22 and MoS_2 FET/anti-CK8 gradually decreases. The decrease of I_{DS} could be explained by the specific binding of negatively charged NMP22 and CK8 with antibodies immobilized on the surface of biosensor. According to the "pH memory theory", the dried proteins retain their ionization state and chargeability as that in the aqueous solution (PBS buffer) [43]. The pH (7.4) of PBS we used is higher than the isoelectric point (pI) of NMP22 (5.53) and CK8 (5.52), and therefore these two investigated proteins are negatively charged at this environment. Consequently, the increase of negatively charged target protein molecules on the n-type MoS_2 channel reduces the effective gate field under positive gate bias conditions, thereby reducing carrier density and I_{DS} [44]. The variation of I_{DS} depends on the amount of target molecules binding on the device surface. Figure 3(c, d) represents the variation of calibrated sensing responses ($\Delta I_{DS}/I_0$) *versus* NMP22 concentration (C_{NMP22}) and CK8 concentration (C_{CK8}). Here, $\Delta I_{DS}/I_0$ refers to the relative I_{DS} change of antibody functionalized MoS_2 sensor before and after binding with target molecules at a fixed V_{GS} of 100 V. From the curve, it also can be seen that the linear working range of our designed MoS_2 sensor for target bladder cancer biomarkers is 10^{-6}–10^{-1} pg mL^{-1} (Figure S3). The limit of detection (LOD) of the MoS_2 FET/anti-NMP22 and MoS_2 FET/anti-CK8 biosensor for NMP22 and CK8 could reach as low as 1 ag mL^{-1}.

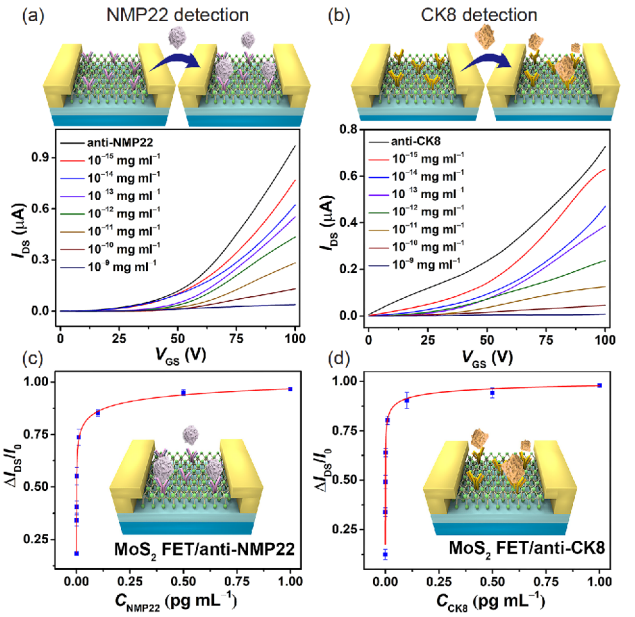

Figure 3 (a, b) Schematic and I_{DS}-V_{GS} response curves of MoS_2 FET sensor array towards NMP22 and CK8. (c, d) The variation of calibrated sensing responses ($\Delta I_{DS}/I_0$, relative change of I_{DS} measured at a fixed V_{GS} of 100 V) *versus* NMP22 and CK8 concentrations. Error bars indicate standard deviation of triplicate tests from different devices. Inset: schematic drawing of the binding of target bladder cancer biomarkers on MoS_2 FET sensor device (color online).

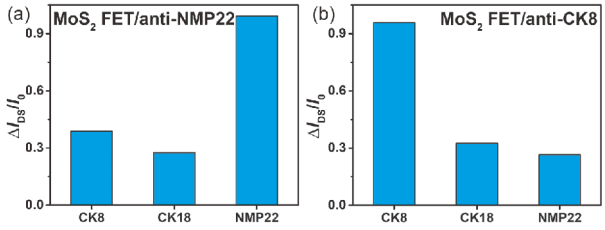

Figure 4 Calibrated sensing responses ($\Delta I_{DS}/I_0$) of (a) MoS_2 FET/anti-NMP22 biosensor and (b) MoS_2 FET/anti-CK8 biosensor towards specific and nonspecific proteins (color online).

3.4 Specificity of MoS_2 FET sensor array

The specificity and selectivity of our MoS_2 FET sensor array were investigated by imposing the corresponding antibody molecules functionalized MoS_2 FET sensor towards specific target protein molecules and nonspecific protein molecules (Figure 4(a, b)). It can be observed that the antibody molecules functionalized MoS_2 FET sensors show a high current response for specific target protein molecules, while the sensing response towards non-target protein molecules is extremely low, suggesting that our designed MoS_2 FET sensor exhibits high selectivity. The excellent sensing performance suggests that our designed MoS_2 FET sensor could be used in highly sensitive and selective quantification of trace amount of bladder cancer biomarkers.

3.5 Application of MoS_2 FET sensor array in human urine samples detection

The clinical applicability of MoS_2 FET sensor array was investigated by detecting the sensing performance of MoS_2 FET sensor array for bladder cancer biomarkers from human urine samples. As illustrated in Figure 5(a), the pretreated urine samples from 3 bladder cancer patients and 3 healthy donors were exposed on the MoS_2 FET sensor array, and the capture of target protein molecules would induce a current variation of MoS_2 FET sensor. The amount of target bladder cancer biomarkers in human urine could be calculated by the calibrated sensing response curves and the fitting equations of $\Delta I_{DS}/I_0$–C_{NMP22} and $\Delta I_{DS}/I_0$–C_{CK8} (Equations S1 and S2, Supporting information online). From Figure 5(b), it can be seen that the concentrations of bladder cancer biomarkers in bladder cancer patients are higher than that of healthy donors, suggesting that the MoS_2 FET sensor could effectively differentiate bladder cancer patients from healthy donors. In order to evaluate the accuracy of the MoS_2 FET sensor array, the recoveries of the measurements were calculated. As shown in Table S1 (Supporting information online), the re-

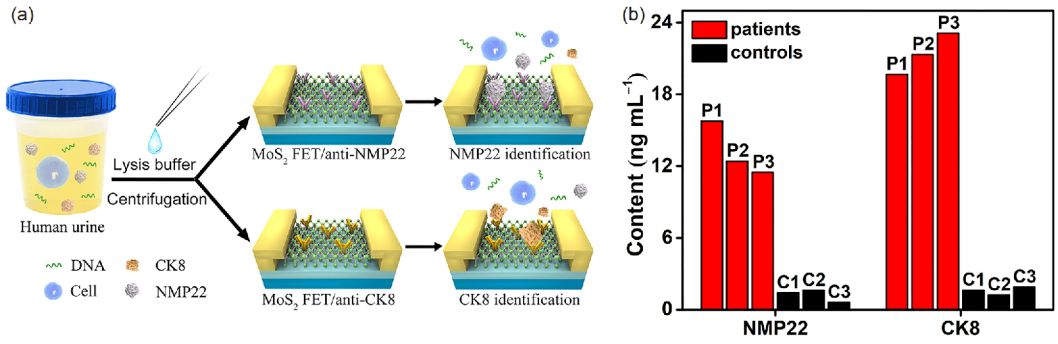

Figure 5 (a) Schematic illustration of the MoS_2 FET sensor array for simultaneous detection of NMP22 and CK8 in human urine samples. (b) The content of NMP22 and CK8 in urine samples from bladder cancer patients and healthy donors measured with MoS_2 FET sensor array. P represents bladder cancer patients and C represents the healthy donors. Nos. 1–3 represent different samples. For example, "P1" represents a urine sample from bladder cancer patient No. 1 (color online).

coveries of our method to detect NMP22 and CK8 were 95.9%–97.3% and 93.1%–104.9%, respectively. The concentrations of NMP22 and CK8 in human urine samples obtained by MoS_2 FET sensor array are in good agreement with the cutoff values of ELISA methods reported in the literatures (Table S2) [45,46]. The applicability of MoS_2 FET sensor array in human urine samples with complex biological environment suggests the potential of MoS_2 FET sensor array in the diagnosis of bladder cancer. To achieve this goal, extensive detection of diverse urine samples and exploration of the differences of the biomarker concentrations in patients with different stages of bladder cancer, patients with benign bladder disease and healthy people combined with clinical diagnosis analysis should be performed systematically in the future work.

4 Conclusions

In conclusion, we constructed a MoS_2 FET sensor array for the quantification of multiple biomarkers of bladder cancer. The MoS_2 FET sensor array exhibits high sensitivity and specificity towards bladder cancer biomarkers. The detection limits of MoS_2 FET sensor array towards NMP22 and CK8 could reach as low as 0.027 and 0.019 aM, respectively. The MoS_2 FET sensor array also shows excellent sensing performance towards human urine samples and could effectively differentiate bladder cancer patients from healthy donors. Our designed high performance MoS_2 FET sensor array suggests a promising approach for the diagnosis of bladder cancer in the future.

Acknowledgements This work was supported by the National Key Research and Development Program of China (2017YFA0208000), the National Natural Science Foundation of China (21925401, 21904033, 21675120), and Changsha Municipal Science and Technology Projects, China (kq1901030).

Conflict of interest The authors declare that they have no conflict of interest.

Supporting information The supporting information is available online at http://chem.scichina.com and http://link.springer.com/journal/11426. The supporting materials are published as submitted, without typesetting or editing. The responsibility for scientific accuracy and content remains entirely with the authors.

1 Frantzi M, van Kessel KE, Zwarthoff EC, Marquez M, Rava M, Malats N, Merseburger AS, Katafigiotis I, Stravodimos K, Mullen W, Zoidakis J, Makridakis M, Pejchinovski M, Critselis E, Lichtinghagen R, Brand K, Dakna M, Roubelakis MG, Theodorescu D, Vlahou A, Mischak H, Anagnou NP. *Clin Cancer Res*, 2016, 22: 4077–4086
2 Burger M, Catto JWF, Dalbagni G, Grossman HB, Herr H, Karakiewicz P, Kassouf W, Kiemeney LA, La Vecchia C, Shariat S, Lotan Y. *Eur Urology*, 2013, 63: 234–241
3 Xiao SH, Wang JF, Xiao N. *Int J Biol Markers*, 2016, 31: e276–e285
4 Pasikanti KK, Esuvaranathan K, Ho PC, Mahendran R, Kamaraj R, Wu QH, Chiong E, Chan ECY. *J Proteome Res*, 2010, 9: 2988–2995
5 Li N, Wang Y, Li Y, Cao W, Ma H, Wu D, Du B, Wei Q. *Sensor Actuat B-Chem*, 2014, 202: 67–73
6 Parikh AR, Leshchiner I, Elagina L, Goyal L, Levovitz C, Siravegna G, Livitz D, Rhrissorrakrai K, Martin EE, van Seventer EE, Hanna M, Slowik K, Utro F, Pinto CJ, Wong A, Danysh BP, de la Cruz FF, Fetter IJ, Nadres B, Shahzade HA, Allen JN, Blaszkowsky LS, Clark JW, Giantonio B, Murphy JE, Nipp RD, Roeland E, Ryan DP, Weekes CD, Kwak EL, Faris JE, Wo JY, Aguet F, Dey-Guha I, Hazar-Rethinam M, Dias-Santagata D, Ting DT, Zhu AX, Hong TS, Golub TR, Iafrate AJ, Adalsteinsson VA, Bardelli A, Parida L, Juric D, Getz G, Corcoran RB. *Nat Med*, 2019, 25: 1415–1421
7 Christensen E, Birkenkamp-Demtröder K, Nordentoft I, Høyer S, van der Keur K, van Kessel K, Zwarthoff E, Agerbæk M, Ørntoft TF, Jensen JB, Dyrskjøt L. *Eur Urology*, 2017, 71: 961–969
8 Costa VL, Henrique R, Danielsen SA, Duarte-Pereira S, Eknaes M, Skotheim RI, Rodrigues A, Magalhães JS, Oliveira J, Lothe RA, Teixeira MR, Jerónimo C, Lind GE. *Clin Cancer Res*, 2010, 16: 5842–5851
9 Yoshioka Y, Kosaka N, Konishi Y, Ohta H, Okamoto H, Sonoda H, Nonaka R, Yamamoto H, Ishii H, Mori M, Furuta K, Nakajima T, Hayashi H, Sugisaki H, Higashimoto H, Kato T, Takeshita F, Ochiya T. *Nat Commun*, 2014, 5: 3591
10 Miller AM, Shah RH, Pentsova EI, Pourmaleki M, Briggs S, Distefano N, Zheng Y, Skakodub A, Mehta SA, Campos C, Hsieh WY, Selcuklu SD, Ling L, Meng F, Jing X, Samoila A, Bale TA, Tsui DWY,

Grommes C, Viale A, Souweidane MM, Tabar V, Brennan CW, Reiner AS, Rosenblum M, Panageas KS, DeAngelis LM, Young RJ, Berger MF, Mellinghoff IK. *Nature*, 2019, 565: 654–658
11 Liu Q, Liu Y, Wu F, Cao X, Li Z, Alharbi M, Abbas AN, Amer MR, Zhou C. *ACS Nano*, 2018, 12: 1170–1178
12 Wood SL, Knowles MA, Thompson D, Selby PJ, Banks RE. *Nat Rev Urol*, 3013, 10: 206–218
13 Liang LG, Kong MQ, Zhou S, Sheng YF, Wang P, Yu T, Inci F, Kuo WP, Li LJ, Demirci U, Wang SQ. *Sci Rep*, 2017, 7: 46224
14 Goodison S, Rosser CJ, Urquidi V. *Mol Diagn Ther*, 2013, 17: 71–84
15 Dey P. *Clinica Chim Acta*, 2004, 340: 57–65
16 Zhuang Y, Zhang M, Chen B, Duan R, Min X, Zhang Z, Zheng F, Liang H, Zhao Z, Lou X, Xia F. *Anal Chem*, 2015, 87: 9487–9493
17 Wang J, Zhang J, Li T, Shen R, Li G, Ling L. *Biosens Bioelectron*, 2019, 131: 143–148
18 Arya SK, Estrela P. *Biosens Bioelectron*, 2018, 117: 620–627
19 Wu D, Wang Y, Zhang Y, Ma H, Yan T, Du B, Wei Q. *Sci Rep*, 2016, 6: 24551
20 Lin Q, Li Z, Yuan Q. *Chin Chem Lett*, 2019, 30: 1547–1556
21 Ma H, Zhang X, Li X, Li R, Du B, Wei Q. *Talanta*, 2015, 143: 77–82
22 Lee MH, Thomas JL, Chang YC, Tsai YS, Liu BD, Lin HY. *Biosens Bioelectron*, 2016, 79: 789–795
23 Tan C, Cao X, Wu XJ, He Q, Yang J, Zhang X, Chen J, Zhao W, Han S, Nam GH, Sindoro M, Zhang H. *Chem Rev*, 2017, 117: 6225–6331
24 Zhang A, Lieber CM. *Chem Rev*, 2016, 116: 215–257
25 Allen B , Kichambare P , Star A. *Adv Mater*, 2007, 19: 1439–1451
26 Li BR, Hsieh YJ, Chen YX, Chung YT, Pan CY, Chen YT. *J Am Chem Soc*, 2013, 135: 16034–16037
27 Yang Y, Yang X, Zou X, Wu S, Wan D, Cao A, Liao L, Yuan Q, Duan X. *Adv Funct Mater*, 2017, 27: 1604096
28 Sarkar D, Liu W, Xie X, Anselmo AC, Mitragotri S, Banerjee K. *ACS Nano*, 2014, 8: 3992–4003
29 Zhang S, Xu H, Liao F, Sun Y, Ba K, Sun Z, Qiu ZJ, Xu Z, Zhu H, Chen L, Sun Q, Zhou P, Bao W, Zhang DW. *Nanotechnology*, 2019, 30: 174002
30 van der Zande AM, Huang PY, Chenet DA, Berkelbach TC, You YM, Lee GH, Heinz TF, Reichman DR, Muller DA, Hone JC. *Nat Mater*, 2013, 12: 554–561
31 Chen W, Zhao J, Zhang J, Gu L, Yang Z, Li X, Yu H, Zhu X, Yang R, Shi D, Lin X, Guo J, Bai X, Zhang G. *J Am Chem Soc*, 2015, 137: 15632–15635
32 Ahmad R, Tripathy N, Park JH, Hahn YB. *Chem Commun*, 2015, 51: 11968–11971
33 Naylor CH, Kybert NJ, Schneier C, Xi J, Romero G, Saven JG, Liu R, Johnson ATC. *ACS Nano*, 2016, 10: 6173–6179
34 Chen M, Nam H, Rokni H, Wi S, Yoon JS, Chen P, Kurabayashi K, Lu W, Liang X. *ACS Nano*, 2015, 9: 8773–8785
35 Duan R, Zhang Z, Zheng F, Wang L, Guo J, Zhang T, Dai X, Zhang S, Yang D, Kuang R, Wang G, He C, Hakeem A, Shu C, Yin P, Lou X, Zeng F, Liang H, Xia F. *ACS Appl Mater Interfaces*, 2017, 9: 23420–23427
36 Jeon J, Jang SK, Jeon SM, Yoo G, Jang YH, Park JH, Lee S. *Nanoscale*, 2015, 7: 1688–1695
37 Huang Y, Guo J, Kang Y, Ai Y, Li CM. *Nanoscale*, 2015, 7: 19358–19376
38 Shan J, Li J, Chu X, Xu M, Jin F, Wang X, Ma L, Fang X, Wei Z, Wang X. *RSC Adv*, 2018, 8: 7942–7948
39 Zhou G, Chang J, Pu H, Shi K, Mao S, Sui X, Ren R, Cui S, Chen J. *ACS Sens*, 2016, 1: 295–302
40 Lee DW, Lee J, Sohn IY, Kim BY, Son YM, Bark H, Jung J, Choi M, Kim TH, Lee C, Lee NE. *Nano Res*, 2015, 8: 2340–2350
41 Ren X, Ma H, Zhang T, Zhang Y, Yan T, Du B, Wei Q. *ACS Appl Mater Interfaces*, 2017, 9: 37637–37644
42 Sánchez-Carbayo M, Urrutia M, Silva JM, Romaní R, García J, Alférez F, González deBuitrago JM, Navajo JA. *Urology*, 2000, 55: 526–532
43 Park H, Han G, Lee SW, Lee H, Jeong SH, Naqi M, AlMutairi AA, Kim YJ, Lee J, Kim W, Kim S, Yoon Y, Yoo G. *ACS Appl Mater Interfaces*, 2017, 9: 43490–43497
44 Gong X, Liu Y, Xiang H, Liu H, Liu Z, Zhao X, Li J, Li H, Hong G, Hu TS, Chen H, Liu S, Yu G. *Sci China Mater*, 2019, 62: 1479–1487
45 Zhou BF, Wei JH, Chen ZH, Dong P, Lai YR, Fang Y, Jiang HM, Lu J, Zhou FJ, Xie D, Luo JH, Chen W. *Oncotarget*, 2016, 7: 41703–41714
46 Kibar Y, Goktas S, Kilic S, Yaman H, Onguru O, Peker AF. *Ann Clin Lab Sci*, 2006, 36: 31−38